Development of a cost effective automated platform to produce human liver spheroids for basic and applied research

Biofabrication

International Society for Biofabrication

Development of a cost-effective automated platform to produce human liver spheroids for basic and applied research

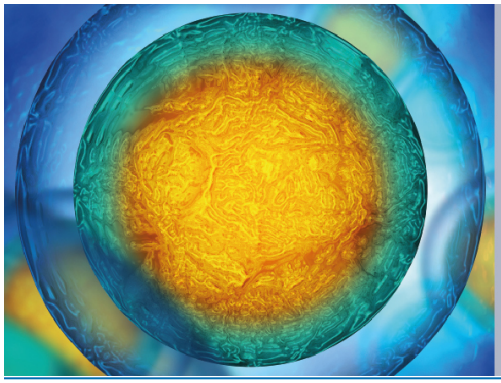

Biofabrication

PAPER

Development of a cost-effective automated platform to produce human liver spheroids for basic and applied research

B Lucendo-Villarin[1,2], J Meseguer-Ripolles[1,2], J Drew[3], L Fischer[1], E Ma[3,4], O Flint[1], K J Simpson[5], L M Machesky[3,4], J C Mountford[6] and D C Hay[1,7]

[1] Centre for Regenerative Medicine, University of Edinburgh, Edinburgh EH16 4UU, United Kingdom
[2] Both authors contributed equally to this manuscript.
[3] CRUK Beatson Institute, Garscube Estate, Switchback Road, Bearsden, Glasgow G61 1BD, United Kingdom
[4] Institute of Cancer Sciences, University of Glasgow, Garscube Campus, G61 1BD, United Kingdom
[5] Scottish Liver Transplant Unit, Royal Infirmary, Edinburgh EH16 4SA, United Kingdom
[6] SNBTS, 52 Research Avenue North, Heriot-Watt Research Park, Edinburgh EH14 4BE, United Kingdom
[7] Author to whom any correspondence should be addressed.

E-mail: davehay@talktalk.net

Keywords: stem cell, liver, hepatocyte, endothelial cell, stellate cell, tissue engineering, automation

Supplementary material for this article is available online

OPEN ACCESS

RECEIVED
8 July 2020

REVISED
29 September 2020

ACCEPTED FOR PUBLICATION
2 October 2020

PUBLISHED
28 October 2020

Abstract

Liver disease represents an increasing cause of global morbidity and mortality. Currently, liver transplant is the only treatment curative for end-stage liver disease. Donor organs cannot meet the demand and therefore scalable treatments and new disease models are required to improve clinical intervention. Pluripotent stem cells represent a renewable source of human tissue. Recent advances in three-dimensional cell culture have provided the field with more complex systems that better mimic liver physiology and function. Despite these improvements, current cell-based models are variable in performance and expensive to manufacture at scale. This is due, in part, to the use of poorly defined or cross-species materials within the process, severely affecting technology translation. To address this issue, we have developed an automated and economical platform to produce liver tissue at scale for modelling disease and small molecule screening. Stem cell derived liver spheres were formed by combining hepatic progenitors with endothelial cells and stellate cells, in the ratios found within the liver. The resulting tissue permitted the study of human liver biology 'in the dish' and could be scaled for screening. In summary, we have developed an automated differentiation system that permits reliable self-assembly of human liver tissue for biomedical application. Going forward we believe that this technology will not only serve as an *in vitro* resource, and may have an important role to play in supporting failing liver function in humans.

1. Introduction

The liver is the largest internal organ performing hundreds of different functions [1]. Parenchymal cells of the liver (hepatocytes) make up approximately 70–80% of the liver's mass and perform most of the metabolic functions. Hepatocytes are highly polarised epithelial cells and their function is supported by the non-parenchymal cells that reside in the liver [2]. Their basolateral surface is in direct contact with sinusoidal endothelial cells, facilitating efficient transfer of substrates between the blood and the liver. The tight junctions between hepatocytes form the apical membrane that collects and transports bile [3]. The organised structure of the liver is key to the organ's ability to perform a myriad of metabolic functions and regenerate when necessary. During liver damage, the loss of this structure, and intimate cell interactions becomes evident, and if uncorrected leads to the development of disease.

Currently, liver disease is a global health issue. Although the liver is a highly regenerative organ, the exposure to serious or repeated injury severely impairs this process. This can lead to reduced organ function and altered physiology, often requiring clinical intervention. While end-stage liver disease can be successfully

treated by organ transplantation, it is an invasive surgical procedure, which is limited by organ donation [4]. Therefore, development of renewable sources of human liver tissue to treat disease are eagerly awaited [4]. In addition to organ and tissue transplantation, human liver tissue has an important role to play in disease modelling and improving the efficiency of the drug development process [5–8].

To date, the field relies on different types of cell-based systems to model human liver biology. Primary human hepatocytes are considered as the gold standard model, however their isolation from diseased tissue, poor scalability and rapid loss of phenotype limits their routine use for modelling studies *in vitro* [9]. Therefore, cancer derived cell lines have been developed and are widely used to study human liver biology 'in the dish', due to their abundance and cost-effective scale-up [10]. Despite their advantages, cell lines offer limited biological relevance when compared to primary human tissue. As a result, researchers have turned their attention to renewable cell-based systems. In particular, pluripotent stem cell technology has been proposed as a suitable alternative to overcome limitations associated with organ scarcity, loss of cell phenotype and routine use of cancer cell lines [11]. A number of efficient hepatocyte differentiation procedures from pluripotent stem cells have been developed (for a literature review see [12]). Those models have been used to study different aspects of liver disease, such as metabolic disorders [13, 14], non-alcoholic fatty liver disease [15, 16], and drug induced liver injury (DILI) [17, 18]. Although proof of concept has been established, further modifications to those models are required to improve data quality and extrapolation toward human physiology [19].

Most liver models used for large-scale experimentation, are two-dimensional (2D) in nature. These simplistic environments are useful, but also lead to non-physiological alterations in many cellular processes, including cytoskeleton formation and extracellular matrix protein production [12]. These alterations have significant impact on cell phenotype and model accuracy [20]. For example, in the case of the liver and drug exposure, changes driven by 2D culture alter hepatocyte polarity and therefore exposure to drugs [21]. Although 2D models do not accurately capture human organ function, recent experimentation demonstrates that significant progress has been made extrapolating simple *in vitro* model data to *in vivo* exposure levels in humans [22].

To improve tissue performance and phenotype, researchers have developed 3D models, which better capture aspects of organ development and structure. In the context of the liver, this approach has been shown to substantially improve cell phenotype and stability *in vitro* [23, 24]. The pioneering studies by Takebe *et al* demonstrated that primary endothelial cells, mesenchymal stem cells and stem cell derived hepatocytes could be used to generate 3D liver like tissue that performed *in vitro* and *in vivo* [25]. More recently, Takebe *et al* built functional liver tissue wholly from human iPSC derivatives, representing a significant advance for the field [26], although the system has not been used for large-scale production as of yet. Alternative approaches to generate functional liver tissue and to better understand multi-lineage communication have also been developed by a number of other groups using self and template-based cell assembly (for a literature review see [12]). Whilst significant advances have been made, key challenges remain to manufacture human liver tissue. Those include intra- and inter-experimental consistency, and cost effective production at scale [12, 27].

While it is clear that human pluripotent stem cells have revolutionary potential for modern medicine [28]. Most procedures published to date rely on undefined and/or xenobiotic materials to expand, differentiate and engineer units of human tissue. The incorporation of these types of materials into the manufacturing process are known to elicit uncontrolled effects that can lead to variable cell performance and therefore batch-to-batch variation. This was recently highlighted as a key limitation to using current organoid systems to study human liver biology [27]. Although these limitations are not huge hurdles for small scale lab-based research, they serve as significant challenges for technology scale-up, process automation and technology translation.

Therefore, the objectives of our study were to build a fully defined stem cell-based tissue engineering platform, that was capable of automation, was transferable between users and could be used to model human liver disease. Our hypothesis was that the combination of defined cellular differentiation, cell self-assembly and engineering processes were essential to achieve this goal. We report the development of a robust and automated tissue-engineering platform to produce 3D human liver tissue at scale and use this to model human disease and perform small molecule screening.

2. Material and methods

2.1. Cell culture and differentiation

2.1.1. Maintenance of human PSCs

Human pluripotent stem cells (hPSC) lines, including two embryonic stem cell lines (H9 and Man12) and an iPSC line (P106) were cultured on Laminin 521 (Biolamina) coated plates in serum-free mTeSR1 ™ (STEMCELL Technologies) in a humidified 37 °C, 5% CO_2 incubator as previously described (Cameron *et al* 2015). Cells were routinely passaged using Gentle Cell Dissociation Reagent (STEMCELL Technologies) and replated as small clumps of cells at a dilution of 1:6–1:10. The cell lines were propagated in

antibiotic free medium and tested regularly for mycoplasma infection.

2.1.2. Hepatic differentiation

For hepatic differentiation, hPSCs were dissociated using Gentle Cell Dissociation Reagent (STEMCELL technologies) and plated onto pre-coated wells with Laminin 521 (BioLamina) in mTeSR1™ supplemented with 10 μM Y-27632 (Biotech) at a density of 40 000 cells cm^{-2}. Differentiation was initiated 24 h post seeding when cell confluency reached 40% by replacing stem cell medium with endoderm differentiation medium [RPMI 1640 containing 1× B27 (Life Technologies), 100 ng ml^{-1} Activin A (Biotech) and 50 ng ml^{-1} Wnat3a (Biotech)]. The medium was changed every 24 h for 3 d. On day 4, endoderm differentiation medium was replaced with hepatic progenitor differentiation medium, and this was renewed every second day for a further 5 d. The medium consisted of knockout (KO)-DMEM (Life Technologies), Serum replacement (Life Technologies), 0.5% Glutamax (Life Technologies), 1% non-essential amino acids (Life Technologies), 0.2% β-mercaptoethanol (Life Technologies), and 1% DMSO (Sigma). On day 9, differentiating cells were cultured in the hepatocyte maturation medium which comprised of Hepato-ZYME (Life Technologies) containing 1% Glutamax (Life Technologies), supplemented with 10 ng ml^{-1} hepatocyte growth factor (PeproTech) and 20 ng ml^{-1} oncostatin m (PeproTech) as described previously [28].

2.1.3. Endothelial cell differentiation

Endothelial differentiation was performed using an adapted a protocol previously described [29]. Briefly, hPSCs were dissociated using Gentle Cell Dissociation Reagent (STEMCELL technologies) and plated onto pre-coated wells with Laminin 521 in mTeSR1™ supplemented with 10 μM Y-27632 (Biotech) at a density of 25 000 cells cm^{-2}. After 24 h the media was replaced with mesoderm priming medium, consisting of N2B27 medium (1:1 mixture of DMEM:F12 and CTS Neurobasal media) supplemented with Glutamax N2 CTS, B27 CTS (Life Technologies), 10 μM CHIR99021 (Tocris) and 25 ng ml^{-1} BMP4 (Biotech). After three days, the priming medium was replaced by endothelial induction medium consisting of StemPro-34 SFM medium (Life Technologies) supplemented with 200 ng ml^{-1} vascular endothelial growth factor (VEGF) (Biotech) and 2 μM forskolin (Sigma-Aldrich). The induction medium was renewed after 24 h.

2.1.4. Hepatic stellate cell differentiation

Hepatic stellate cell differentiation was achieved using an adapted protocol previously described [30]. Briefly, hPSC were dissociated using Gentle Cell Dissociation Reagent (STEMCELL technologies) and plated onto pre-coated wells with Laminin 521 in mTeSR1 ™ supplemented with 10 μM Y-27632 (Biotech) at a density of 75 000 cells cm^{-2}. Differentiation was initiated 24 h post seeding by replacing stem cell medium with hepatic stellate cell (HSC) differentiation medium [57% DMEM low glucose (ThermoFisher), 40% MCDB-201-water (Sigma), 0.25× linoleic acid-bovine serum albumin (Sigma), 0.25× insulin-transferrin-selenium (Sigma), 1% penicillin streptomycin (ThermoFisher Scientific), 10^{-4} M L-ascorbic acid (Sigma), 2.5 μM dexamethasone (Sigma) and 50 μM 2-mercaptoethanol (Life Technologies)]. Medium was changed every 48 h. Growth factors (Biotech) were added as follows: 20 ng ml^{-1} BMP4 from days 0 to 4, 20 ng ml^{-1} FGF1 and 20 ng ml^{-1} FGF3 from days 4 to 8, 50 μM retinol (Sigma) and 100 μM palmitic acid (Sigma) were added from days 6 to 12.

2.1.5. Formation and maintenance of self-aggregated liver spheres

Agarose microplates were manufactured in 256-well format using the 3D Petri Dish mould (Sigma Aldrich) and transferred to 12-well plates (Corning) as previously described [31]. hPSC-derived somatic cells were incubated with 1 ml/10 cm^2 of TrypLE express (ThermoFisher) for 5–20 min at 37 °C, dependent on the cell type. Following this, the reaction was stopped by adding the same volume of liver sphere medium supplemented with 10 μM Y-27632 (Biotech). After detaching, hPSC-derived hepatic progenitor cells and hepatic stellate-like cells were filtered to get a single cell suspension using a 30 μm cell strainer (Sarstedt) and then centrifugated at 1500 rpm for 10 min. Liver sphere medium consisted of a 1:1 mixture of William's E media and SFM-Endothelial media with 5% Serum replacement (ThermoFisher), 1% Glutamax and 1% penicillin-streptomycin (ThermoFisher). The cell pellet was resuspended in liver sphere medium, supplemented with 10 μM Y-27632 (Biotech), 10 ng ml^{-1} EGF (Biotech), 10 ng ml^{-1} FGF (Peptrotech), 10 ng ml^{-1} HGF (Peprotech), 20 ng ml^{-1} OSM (Peprotech) and 50 ng ml^{-1} VEGF (Biotech) at a density of 7,68 × 10^6 live cells ml^{-1} for hepatic progenitor cells and 7.68 × 10^5 live cells ml^{-1} for hepatic stellate-like cells. Post-detachment, hPSC-derived endothelial-like cells were magnetic-associated cell sorting (MACS) enriched using CD144 MicroBeads (Myltenyi Biotec) and resuspended in growth factor and Y-27632 supplemented liver sphere medium at a density of 5.12 × 10^6 live cells ml^{-1}. The agarose microplates were seeded by transferring 190 μl of a solution containing the different cell types at the ratio of 10:3:1 (hepatic progenitor:endothelial cell:stellate cell). After 2–3 h, 1.5 ml of growth factor supplemented liver sphere medium was gently added to each well of 12-well plate. Media was replaced every 48 h.

2.1.6. Automated production of liver spheres

Following hPSC differentiation and cell detachment and endothelial enrichment, a cell mixture containing 1 volume of hepatic progenitor cells solution at 10.95×10^6 live cells ml^{-1}, 0.5 volume of endothelial-like cells solution at 7.3×10^6 live cells ml^{-1} and 0.5 volume of HSCs at 2.19×10^6 live cells ml^{-1} (or same volume of media in the absence of a cell type) was prepared to a final cell ratio of 10:3:1 (HB:ELC:HSC). The multidrop system (ThermoFisher 5840300) was employed to dispense the cell solution into a 'V' shape 96 well plate. A Viaflo 96 head pipette system (Integra 6001) was employed to seed 40 μl of cell containing solution to each well of a 96 well-hydrogel array containing 73 microwells of 500 μm, per well (Gri3D, Sunbiosciences). Once liver spheres were aggregated, 200 μl of liver sphere medium was added into the feeding chamber with using the Viaflo 96 head pipetting system (Integra 6132). Media changes were performed every 48 h using both the multidrop and Viaflo.

2.1.7. Cancer cell co-culture assay

Hepato-endothelial (HE) liver spheres 4 weeks post-aggregation were used for co-culture assays with cancer cell lines. Single cell suspensions of MIAPaCa-2 (a pancreatic ductal adenocarcinoma cell line) and PDAC (Pancreatic ductal adenocarcinoma cell line)-A (Mouse KPC PDAC cell line) were labelled with CellTracker Red dye (ThermoFisher, C34552) as per manufacturer's instructions prior to plating 5×10^4 cells into polyHEMA-coated 96-well plates containing HE liver spheres in liver sphere medium. After 24 h, samples were fixed, stained with Alexa Fluor-488 Phalloidin, and embedded in 1% agarose. *Z*-stack tile scans of each well were imaged with an Opera Phenix™ High-Content Screening system and interactions between cancer cells and liver spheres scored in ImageJ. PANC1 cells were purchased from ATCC (American Type Culture Collection) and PDAC-A cells were derived from mice with tumours expressing KRas ^{G12D} and P53 ^{R172H} gifted from Dr S Karim and Dr J Morton at the Beatson Institute.

2.2. Phenotypic and functional characterisation

2.2.1. Immunofluorescence

Liver spheres were fixed for at least 1 h in 4% neutral buffered formalin solution (pH 7.4) at 4 °C and washed twice with PBS at room temperature before embedding in agarose. Agarose-embedded liver spheres were then embedded in paraffin and sectioned at 4 μm. Antigen retrieval was performed by heating dewaxed and rehydrated sections in 1× Tris–EDTA buffer solution for 7 min in microwave. Washed slides were used for subsequent staining. To stain sectioned spheres, stem cell derived tissue was blocked with 10% BSA in PBS-tween and incubated with primary antibody overnight at 4 °C. The primary antibody was detected using species-specific fluorescent-conjugated secondary antibody. Sections were counterstained with NucBlue Hoechst 33342 (Sigma-Aldrich) and mounted with Fluoromount-G (SouthernBiotech) before microscopy. Images were taken using a Nikon Eclipse e600 microscope equipped with a Retiga 2000 R camera (Q-Imaging) and Image-Pro Premier software. Antibodies used are listed in supplementary table 1

For whole mount staining liver spheres were fixed using 4% PFA for 30 min. Following fixation, cells were washed three times with 1× PBS. Liver spheres were stained with Bodipy 493/503 (1:2000) and NucBlue Live ReadyProbes® Reagent (1 drop ml^{-1}) and incubated 4 h at RT in the dark. Following staining, three 1× PBS washes were performed and liver spheres were transferred into an ibidi μ-Slide 8 Well chamber and resuspended into a 60% (vol/vol) glycerol and 2.5 M fructose clearing solution [32]. Images were taking with the Confocal microscope Nikon A1-R HD25 using a Plan Apo λ 20× objective, Nikon A1 LFOV camera and 0.95 μm *Z*-step.

2D cell cultures were fixed in 100% ice-cold methanol at −20 °C for 30 min. Following this, cells were washed twice with 1× PBS at room temperature. Cell monolayers were blocked with PBS-0.1% Tween containing 10% BSA for 1 h, and the monolayers were incubated with primary antibodies diluted in PBS-0.1% Tween/1% BSA at 4 °C overnight. The following day, the primary antibody was removed, and the fixed monolayers were washed three times with 1× PBS-0.1% Tween/1% BSA. Following this, the cells were incubated with the appropriate secondary antibody diluted in PBS/0.1% Tween/1% BSA for 1 h at room temperature and washed three times with 1× PBS. Cultures were then mounted with PermaFluor aqueous mounting medium (Thermo Scientific) and counterstained with NucBlue Hoechst 33342 (Sigma-Aldrich). The cells were imaged with an Axio Observer Z1 microscope with LD PlanNeoFluar objective lenses (Carl Zeiss). This microscope was coupled to a Zeiss AxioCamMR3 camera used for image acquisition. The images were processed through Zeiss Axiovision SE 64 Rel 4.8, with Zeiss Axiovision version 4.9.1.0 used to analyse the images. The percentage of positive cells and SD was calculated from eight fields of view.

2.2.2. High content imaging and analysis

Image acquisition was performed using the automated Operetta fluorescent microscope. In brief, plates were placed in the Operetta and a single image at 2× was acquired to image most of the well surface. Sphere segmentation for image analysis was performed using the Columbus image analysis software. Texture-based pixel classification was employed for background removal by selecting multiple examples of selected pixels and background pixels. Next, an inverted image was used for sphere identification based on sphere size and texture. Finally, a

quality control step using object classification was employed for sphere selection. This was performed so that properly segmented spheres were analysed. Finally, object count and morphology quantification were employed for sphere count and area quantification.

2.2.3. Flow cytometry

Single-cell populations were resuspended in FACS (Fluoresecent Activated Cell Sorting)-PBS (PBS containing 0.1% BSA and 0.1% sodium azide). The cells were counted and diluted to a density of 1×10^6 viable cells ml^{-1}. A total of 2×10^5 cells were incubated for 30 min at 4 °C with conjugated antibodies to CD144 (BD Biosciences, 1:40 dilution), CD31 (eBiosciences, 1:100 dilution), CD166 (BD Biosciences, 1:100 dilution) or CD140b (BD Biosciences, 1:40 dilution). Cells were washed twice in FACS-PBS. Cells incubated with isotype controls were included as control and dead cells and debris were excluded from the analysis based on scatter characteristics. Data for at least 10 000 live events were acquired for each sample using a BD LSR Fortessa cytometer and were analysed using FlowJo version V10 software (FlowJo LLC). Data are presented as percentage positive staining.

2.2.4. Protein secretion

To measure alpha-fetoprotein and albumin secretion, liver spheres were maintained in supplemented liver sphere medium without SFM-Endothelial media and in the presence of 10 μM hydrocortisone 21-hemisuccinate sodium salt. Culture media was collected after 24 h and quantified using commercially available ELISA kits (Alpha Diagnostic International). Data were normalised by total protein content measured using bicinchoninic acid (BCA) assay (ThermoFisher). Protein secretion in 2D hepatocyte like cells (HLCs) cultures was performed as previously described [28].

2.2.5. Cytochrome P450 activity

To measure Cyp3A and Cyp1A2 activity, 50 μM of Luciferin-PFBE substrate (Promega) or 100 μM of Luciferin-ME (Promega) were incubated with liver spheres maintained in liver sphere medium. Cytochrome P450 activity was measured 24 h later using the P450-Glo assay kit (Promega) according to manufacturer's instructions. Cytochrome P450 activity in 2D HLCs cultures was performed as previously described [28].

2.2.6. Exposure to signalling pathway inhibitors

The selective small molecule inhibitors for the c-Met receptor (Mesylate), the VEGF receptor 1, 2 and 3 (axitibin), for the VEGF receptor 2 (DMH4) and the glycoprotein (gp) 130 receptor (Sc144) were all purchased from Tocris. They were resuspended in dimethyl sulphoxide, DMSO (Sigma Aldrich) and diluted 1:1000 in liver spheroid medium according to the manufacturers recommended IC_{50} concentrations. Melysate was employed at 7 nM, axitibin was employed at 0.2 and 1.2 nM, DMH4 was employed at 161 nM and SC144 was employed at 720 nM. Inhibitors and the controls were added to liver sphere cultures for the denoted time points. Fresh inhibitors and medium were added every 48 h.

2.2.7. Assessment of cytochrome P450 metabolism

To assess metabolic activity, stem cell derived liver spheres were incubated with compounds that are metabolised by specific cytochrome P450 enzymes. BMS-872397-01 was selective for Cyp2C19, BMS-808565-01 and BMS-809506-01 were selective for Cyp2C9, BMS-827278-01 and BMS-835981-01 were selective for Cyp2D6 and BMS-707756 was selective for Cyp3A4. BMS (Bristol Myers Squibb) compounds were diluted in dimethyl sulphoxide, DMSO (Sigma Aldrich) to obtain a 1000× stock concentration (50 mM) and were subsequently diluted 1:1000 in supplemented liver spheroid medium and applied to the cells for 72 h at 37 °C in 5% CO_2. Cell viability was measured using RealTime-Glo MT Cell Viability Assay (Promega) following the manufacturer's instructions, at 72 h post exposure. Results were normalised by protein content measured using BCA assay (ThermoFisher) and compared to cell viability in the presence of the vehicle control.

2.2.8. Cell viability in response to healthy and diseased blood plasma

To assess the response of the stem cell derived liver spheres to a clinically relevant situation, spheres exposed to 20% of human plasma serum isolated from patients with paracetamol overdose, for 48 h. Cell viability was measured using RealTime-Glo MT Cell Viability Assay (Promega) following the manufacturer's instructions and determined at 48 h post exposure. Results were normalised by total protein content measured using BCA assay (ThermoFisher) and compared to cell viability in the presence of 20% healthy human serum (Sigma Aldrich).

2.2.9. Liver sphere paracetamol exposure

Paracetamol (Sigma-Aldrich) was prepared as a 4 M stock in DMSO and diluted in liver spheroid medium to 10 mM. At day 17, liver spheres were exposed to paracetamol (10 mM) for 48 h in the incubator at 37 °C. Cell viability was measured using RealTime-Glo MT Cell Viability Assay (Promega) following the manufacturer's instructions and determined after 48 h post exposure.

2.2.10. Oil Red O staining and quantification

The oil red O (ORO) stock solution was prepared by diluting 0.5 g of ORO in 100 ml isopropanol and filtered. ORO working solution was prepared by diluting 30 ml of stock solution with 20 ml of distilled water. Following lactate, pyruvate and octanoate

(LPO) treatment, spheres were fixed using 4% PFA for 30 min. Following fixation, three 1× PBS washes were performed. Following this, liver spheres were washed with 60% isopropanol followed by incubation in the ORO working solution for 15 min at RT, with regular shaking. After staining, multiple washes with 60% isopropanol were performed until clear. Next, liver spheres were transferred into a 1.5 ml tube and 150 μl of isopropanol transferred into the tube to elute the ORO from the spheroids (30 min with shaking at RT). Each sample was centrifuged at 10 000 rpm for 5 min and 50 μl of the solution were transferred (in triplicate) into a clear 96-well plate and measured at an absorbance of 490 nm. Protein quantification was performed using BCA assay.

2.2.11. LPO treatment

Liver spheres were exposed to sodium l-lactate (20 mM), sodium pyruvate (2 mM) and octanoic acid (4 mM) (all Sigma, Gillingham, UK) for 48 h to induce fat loading as previously described [16].

2.2.12. Cytokine detection

Cytokines were quantified from cell culture supernatant using a V-PLEX Human CRP Kit and a U-PLEX Biomarker Group 1 (hu) Assays (Meso Scale Discovery) following the manufacturer's instructions. Twenty five microlitres of liver spheroid supernatant was used for detection. The plate was read on a QuickPlex SQ 120 analyser (Meso Scale Discovery).

2.2.13. Ethics

Ethical approval was from Scotland A Research and Ethics committee. Patients or their nominated next of kin provided informed consent to blood sampling and analysis. Peripheral blood samples were obtained on the day of admission to the Scottish Liver Transplant Unit. Serum was collected after centrifugation and stored at −80 °C until thawing for the experiments. The patient's clinical measurements are summarised in supplementary table 1.

3. Results

3.1. Generation of pure populations of stem cell derived hepatic progenitors and endothelial cells for tissue engineering

Stem cell derived hepatic progenitor cells were produced using a well-defined differentiation process (figure 1(A) [28]). Stem cell morphology progressively changed throughout the differentiation process, culminating in the acquisition of cobblestone morphology (figure 1(B)). Stem cell derived hepatic progenitor populations were homogeneous with cells expressing cytokeratin 19 (99% ± 0.8), HNF4α (98% ± 1.7), alpha-fetoprotein (92.8% ± 1.2) and albumin (39% ± 4.1) (figure 1(C)) and demonstrated the capacity to form functional HLCs (supplementary figure 1 (available online at https://stacks.iop.org/BF/13/015009/mmedia)).

Stem cell derived endothelial like cells (ELCs) were produced using a modified version of an established procedure (figure 1(D) [29],). Again, we observed significant changes in cell morphology as pluripotent cell differentiation proceeded (figure 1(E)). ELC populations were not as homogeneous, ranging from 41% to 64% purity (supplementary figure 2). Therefore, MACS enrichment for CD144 was employed, resulting in a homogeneous population of endothelial cells positive for CD144 and CD31 (on average 95.3% ± 3.6) (figure 1(F)). Following basic characterisation, hepatic progenitor cells in combination with ELCs were aggregated (3:1 ratio) using agarose multi-well technology (figure 1(G)) allowing the production of homogeneous liver spheres (HE) with an average size of 288 μm, (±20.04 μm) (figure 1(H)).

3.2. Characterisation of stem cell derived liver sphere structure and function

Following formation, HE liver sphere structure and function were studied. To understand sphere structure, liver spheres were fixed 2 weeks post-aggregation, embedded and sections cut for immunostaining. We employed the hepatocyte markers, E-Cadherin and HNF4α, and the endothelial markers, VE-Cadherin and CD31, to investigate multicellular organisation and interaction between hepatocytes and endothelial cells (figure 2(A)). Within the sphere, hepatocytes were positioned in the outer layer, surrounding endothelial tubular structures. In addition to endothelial markers, mesenchymal status was confirmed by vimentin localisation with CD31 (figure 2(A)). To gain insight on sphere architecture, whole mount staining was performed to assess hepatocyte and endothelial structure by staining for HNF4α and CD31. Whole sphere imaging revealed CD31 positive endothelial tubes radiated from the centre of the sphere toward the outer layers (supplementary movie 1).

In addition to protein expression, we also studied cytochrome P450 1A2 and 3A metabolism at different time points. Cyp1A2 activity increased during time, from 101416 ± 126986 RLU ml^{-1} mg^{-1} protein (week 1) to $1.63 \times 10^6 \pm 610596$ RLU ml^{-1} mg^{-1} protein (week 4). Cyp3A activity also increased during this period of time, from 15010 ± 6147 RLU ml^{-1} mg^{-1} protein (week 1) to 578958 ± 311661 RLU ml^{-1} mg^{-1} protein (week 4) (figure 2(B)). We successfully obtained hepatic progenitor cells (supplementary figure 1) and ELCs (supplementary figure 2) and formed HE liver spheres from two other pluripotent stem cell lines. Both H9 and Man12 derived liver spheres displayed Cyp 1A2 and 3A activity (supplementary figure 3). The secretion of two liver proteins, albumin and alpha-fetoprotein, was also studied. At week 1 liver spheres secreted

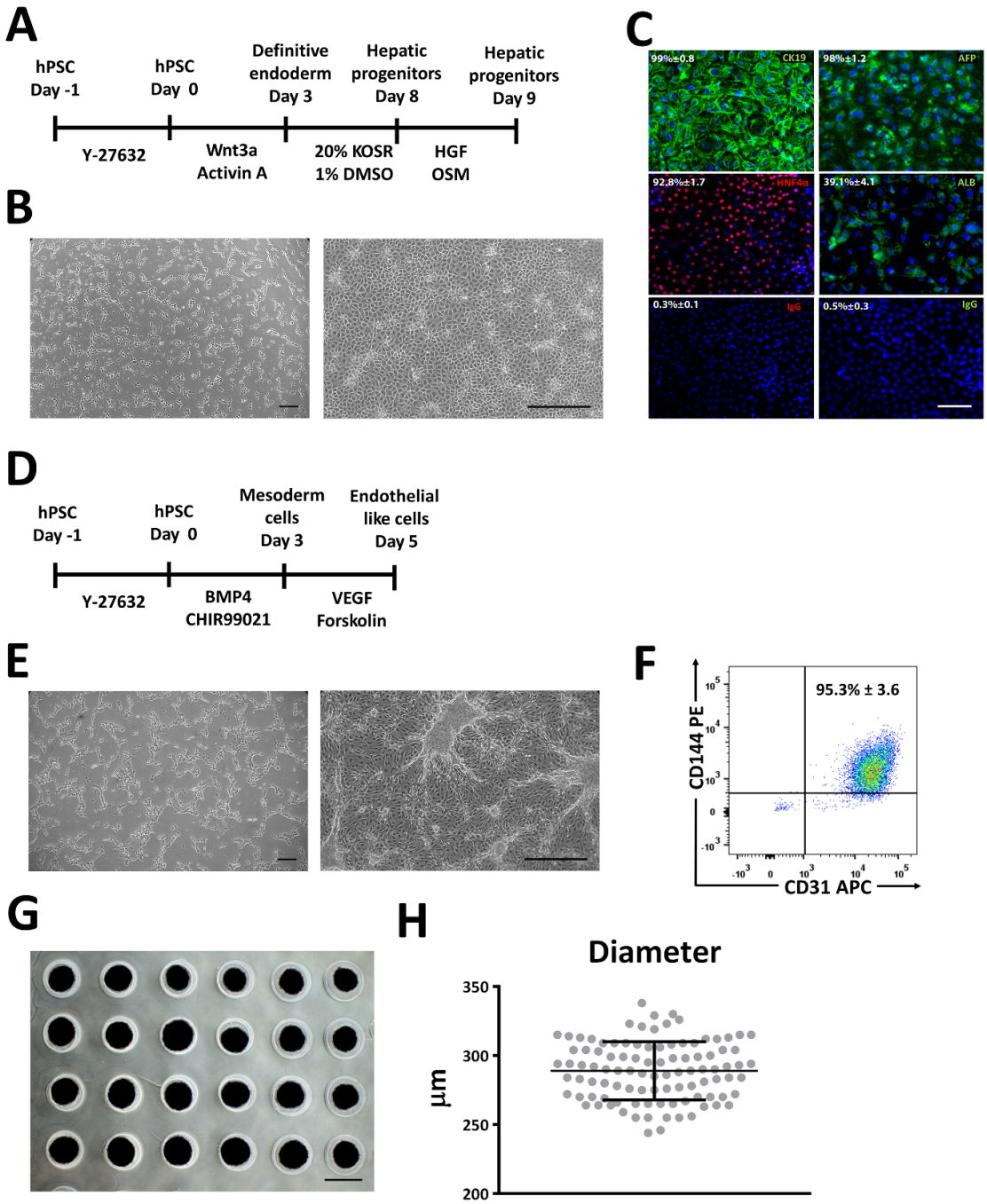

Figure 1. Pluripotent stem cell differentiation and liver sphere formation. (A) Schematic representation of the protocol used to differentiate hPSCs to hepatic progenitor cells. (B) Phase contrast images of representative fields of view of hPSC at the start of the differentiation (left) and at the hepatic progenitor stage (right). Images of hPSC were taken at ×4 magnification and the scale bar is 200 μm. Images of endothelial like cells were taken at ×10 magnification and the scale bar is 100 μm (C) Hepatic progenitor cell immunostaining for AFP, albumin, cytokeratin 19 and HNF4α on hepatic progenitor cells. IgG antibodies were used to demonstrate staining specificity. For each marker, five random fields of view containing at least 400 cells were counted. Images were taken at ×20 magnification and the scale bar represents 100 μm. (D) Schematic representation of the protocol used to differentiate hPSCs to early endothelial cells. (E) Phase contrast images of representative fields of view of hPSC at the start of the differentiation (left) and at the endothelial stage (right). Images of hPSC were taken at ×4 magnification and the scale bar is 200 μm. Images of endothelial like cells were taken at ×10 magnification and the scale bar is 100 μm (F) Representative result following MACS-mediated enrichment for CD144 expressing cells analysed by flow cytometry (mean ± SD, $n = 4$). (G) Phase contrast images of representative fields of view of agarose microwells containing liver spheres 24 h post-aggregation. Images were taken at ×4 magnification and the scale bar represents 400 μm. (H) Size distribution of liver spheres (mean ± SD, $n = 100$). Abbreviations: HNF4α-Hepatocyte Nuclear Factor 4α, AFP-alpha-fetoprotein, CK19. Cytokeratin 19, ALB-Albumin, IgG-Immunoglobulin G.

3149 ± 746 ng ml^{-1} mg^{-1} protein of albumin and the production did not significantly change by week 4 (2983 ± 1472 ng ml^{-1} mg^{-1} of protein). Alpha-fetoprotein secretion displayed a similar trend with no statistically significant variations between week 1 (5858 ± 974 ng ml^{-1} mg^{-1} protein) and week

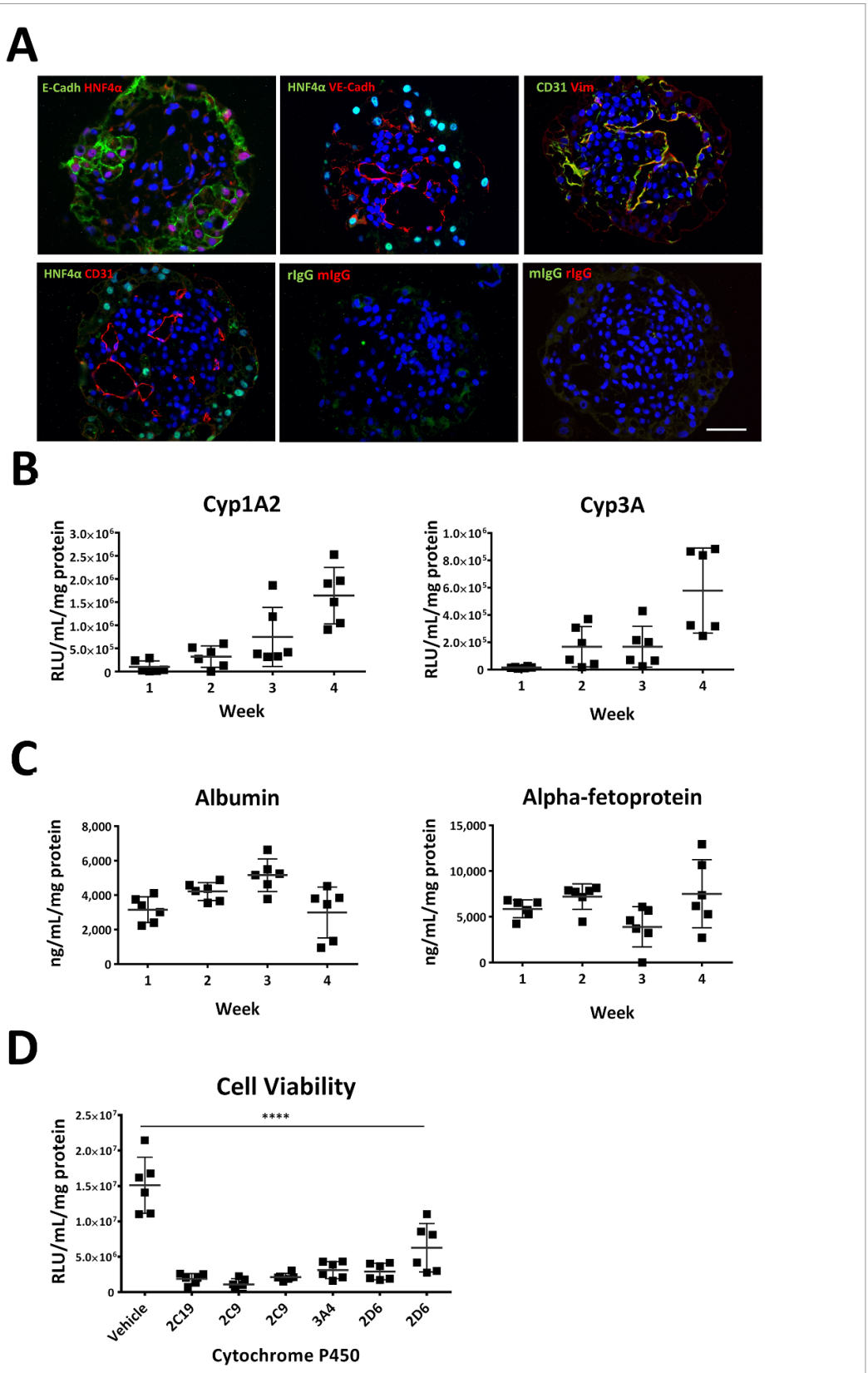

Figure 2. Liver sphere phenotypic characterisation. (A) Immunofluorescent images of liver spheres staining E-Cadherin and HNF4α (hepatocytes) and CD31, VE-Cadherin and Vimentin (endothelial cells). IgG antibodies were used throughout to demonstrate staining specificity. Images were taken at $\times$20 magnification and the scale bar is 120 μm. (B) Cytochrome P450 1A2 and 3A activity were analysed at different time points during liver sphere culture (mean $\pm$ SD, $n = 6$). (C) Secretion of the serum proteins albumin and alpha-fetoprotein were measured by ELISA at the denoted times (mean $\pm$ SD, $n = 6$). (D) ATP depletion in liver spheres exposed to compounds metabolised by specific cytochrome P450 enzymes to toxic endpoints. Data was compared to vehicle control and analysed using the one-way analysis of variance (ANOVA) and Dunnett's multiple comparison test ($\alpha = 0.05$) (mean $\pm$ SD, $n = 6$). Abbreviations: HNF4α-Hepatocyte Nuclear Factor 4α, E-Cadh-E-Cadherin, VE-Cadh-Vascular endothelial cadherin, Vim-Vimentin, IgG-Immunoglobulin G.

4 (7318 ± 3715 ng ml^{-1} mg^{-1} protein) (figure 2(C)). Longer term culture of HE liver spheres resulted in a decreased secretion of alpha-fetoprotein. Week 7 liver spheres secreted 427 ± 146 ng ml^{-1} mg^{-1}, this was reduced to 175 ± 54 ng ml^{-1} mg^{-1} protein at week 10. By week 14 alpha-fetoprotein secretion decreased to 53 ± 34 ng ml^{-1} mg^{-1} protein (supplementary figure 4). Further metabolic characterisation was performed employing a set of training compounds which assess adult Cyp P450 drug metabolising activity. The compounds used, are metabolised by the specific cytochrome P450 enzyme to toxic endpoints, reducing cell viability. Therefore, Cyp P450 activity can be inferred by decreased ATP production. Incubation of liver spheres with those these compounds for 72 h resulted in sphere destruction and significant ATP depletion, ranging from 41% to 90%, dependent on the substrate used (figure 2(D)).

3.3. Liver sphere exposure to high energy substrates, paracetamol, blood plasma and cancer cell aggregates

After liver sphere characterisation, their ability to model disease was tested. Firstly, the ability of liver spheres to store fat was examined following exposure to high energy substrates [16]. Following 48 h LPO exposure, we incubated liver spheres with BODIPY to stain for lipid droplets. We observed an increase in the BODIPY staining in liver spheres exposed to LPO (figure 3(A)). Lipid accumulation was further supported and quantified by Oil red O staining. We observed a 3.4-fold increase in lipid staining compared to the vehicle control (figure 3(B)) .

Following fat loading, we wished to study DILI. For these studies, we used, a common analgesic which can cause severe liver damage when taken above the recommended dose. Exposure to 10 mM of paracetamol resulted in approximately 50% reduction in the ATP levels (figure 3(C)) which is in line with the primary human hepatocytes [33]. To further investigate the ability of the spheres to sustain liver function following DILI, we exposed the liver spheroids to plasma isolated from patients following paracetamol overdose. After 48 h exposure we measured cell viability. We detected significant ATP depletion following exposure to patient sera compared to a heathy control. However, liver sphere structure was maintained following exposure, suggesting that this model could be used to study liver damage and regeneration in future experiments (figure 3(D), supplementary table 1).

The liver is a common site of metastasis for many cancers, including pancreatic and colon cancer, and liver metastases are associated with poor patient prognosis [34, 35]. 3D culture systems have the potential to recapitulate *in vivo* cancer cell–liver niche interactions in a controlled environment and are amenable to mechanistic studies. To investigate the potential of liver spheres as a model of liver metastasis, single cell suspensions of two pancreatic ductal adenocarcinoma cell lines (MIAPaCa-2 and PDAC-A) were co-cultured with liver spheres for 24 h, prior to fixation and whole-mount imaging. Both cancer cell lines spontaneously formed spheroids in suspension, but also interacted with HE liver spheres (figure 3(E)). Interactions often involved a close, flattened surface between two spheres (termed 'Touching') but also instances where cancer cells disrupted the boundary of liver spheres (termed 'Invading') (figure 3(E), right panels). Blind scoring of these interactions revealed that roughly 50% of HE spheres interacted with cancer cells, and suggested the PDAC-A cells were more invasive (Invading; PDAC-A: 13.3%, MIAPaCa-2: 4.5%), in agreement with this cell line's high liver metastatic potential [36] (figure 3(F)). Thus, HE liver spheres show differential interactions with cancer cell lines supporting their potential use as a model of the metastatic niche.

3.4. Automated production of human liver spheres

Blood vessel remodelling and stability in the liver requires the presence of the pericyte [37]. Therefore, in order to improve model physiology we introduced hepatic stellate cells (HSCs), differentiated from pluripotent stem cells [38] (supplementary figure 5(A)). In vitro derived HSCs displayed mesenchymal morphology (supplementary figure 5(B)) and were homogenous, expressing the HSC markers, platelet-derived growth factor (PDGF) Rβ (98.1% ± 2.1) and ALCAM (97.2% ± 1.6) (supplementary figure 5(C)).

To improve technology scale-up and reduce variation, we transferred our manual aggregation system to an automated platform (figure 4(A)). Following differentiation and quality control, the liquid handling dispenser was used to prepare the cell combination. Following this, an automatic pipetting system was employed to dispense cells into microwell plates for self-aggregation. This system was also used for sphere maintenance and for downstream applications. Plate imaging and sphere quantification was carried out 48 h post-seeding using an Operetta high-content imaging system (figures 4(B) and (C)). Analysis was performed using Columbus software and revealed consistency in sphere number per well between columns, with a median of 70 segmented spheres per well (figure 4(D), supplementary figure 6). Cell function was measured analysing cytochrome P450 1A2 activity in HE and hepato-endothelial-stellate (HES) liver spheres. Cyp 1A2 activity increased with time in culture and was significantly higher by week 4 (figure 4(E)). Notably automated manufacture reduced the standard deviation by >2-fold when compared to agarose microwell experiments (figures 2 vs. 4).

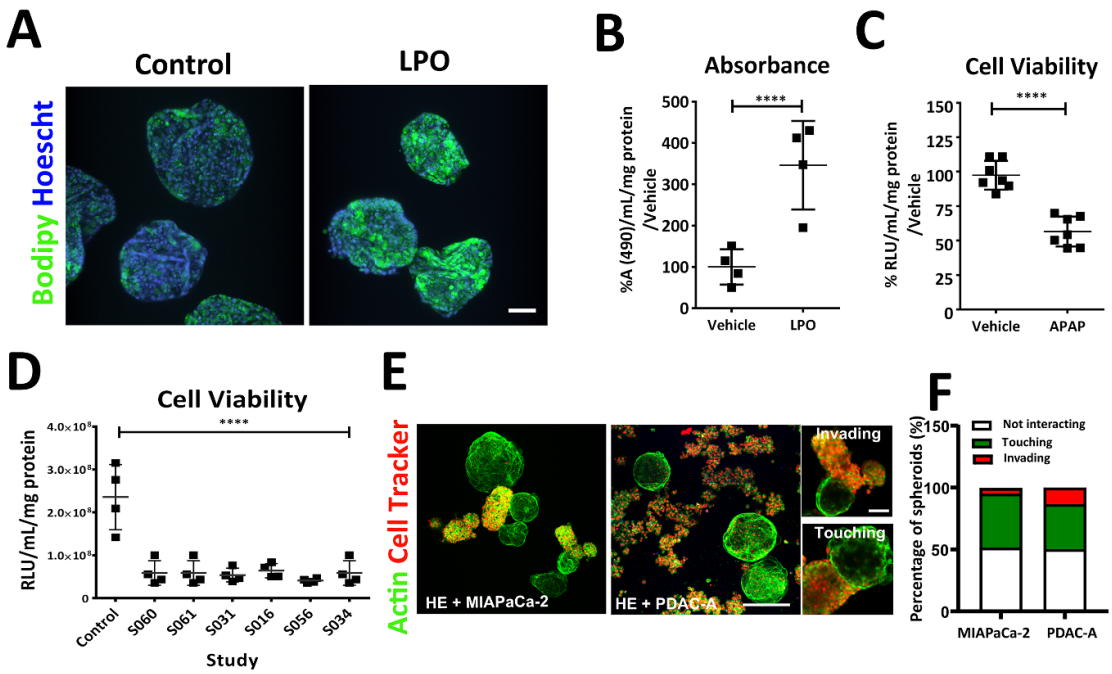

Figure 3. Liver spheres model clinically relevant situations. (A) Immunofluorescence images of liver spheres staining positive for fat droplets (Green-bodipy stain) following exposure to lactate, pyruvate and octanoate (LPO) treatment. (B) Oil red O quantification of liver spheres fat loading after LPO treatment. Data was compared to liver spheres exposed to vehicle control and analysed using unparied *t*-test (mean ± SD, $n = 4$). (C) Liver sphere ability to metabolise paracetamol to toxic by-products was examined and cell viability measured by ATP synthesis. Data was compared to liver spheres exposed to vehicle control and analysed using unpaired *t*-test (mean ± SD, $n = 7$) (D) Exposure to fulminant liver plasma, isolated from patients hospitalised from paracetamol overdose, was assessed measuring ATP synthesis. Data was compared to hepatospheres exposed to healthy control serum. Analysis was performed using with a one-way analysis of variance (ANOVA) ($\alpha = 0.05$) and Dunnett's multiple comparison test (mean ± SD, $n = 4$). (E) Liver sphere interaction with two pancreatic cancer cell lines (MIAPaCa-2 and PDAC-A). Representative maximum intensity projections of liver spheres cultured with pancreatic cancer cells. Right panels show different types of interactions observed. (F) Scoring of interactions of MIAPaCa-2 and PDAC-A cells with HE spheres. Abbreviations: APAP-paracetamol.

3.5. Liver sphere screening to determine essential signalling requirements for tissue self-assembly, function and maintenance *in vitro*

To study the signalling requirements for tissue self-assembly, function and maintenance, we performed a screen. Inhibitors that modulated signalling pathways important to liver development and regeneration were employed (figure 5 and supplementary figure 7). For this purpose, hepatospheres (H), HE and HES liver spheres were self-aggregated in the presence of the specific inhibitors for 2 and 4 weeks, with cell culture medium replenished every 2 d. At the end of the experiments, we used high-content analysis (supplementary figure 6) to segment and calculate the size and number of spheres. Cyp P450 metabolic activity was assessed as before (figure 5 and supplementary figure 7).

Reduced c-Met signalling did not change the number of H, HE or HES liver spheres formed (figure 5(A), supplementary figure 7(A)). However, sphere size was significantly reduced when the c-Met receptor was inhibited in H, HE and HES spheres at 2 weeks post-treatment, but not 4 weeks (figure 5(B), supplementary figure 7(B)). In response to gp130 receptor inhibition, we did not observe a reduction H, HE or HES sphere number (figure 5(A), supplementary figure 7(A)). However, liver sphere size was reduced in HES liver spheres at 2 weeks and in all spheres after 4 weeks (figure 5(B), supplementary figure 7(B)). In response to VEGFR inhibition, H sphere numbers were reduced after treatment with the VEGFR 1–3 inhibitor for 4 weeks (supplementary figure 7(A)). HE and HES, but not H sphere size were increased in response to VEGFR-2 inhibition at the 4 week time point (supplementary figure 7(B)).

Following this, we examined sphere metabolic function following inhibitor exposure. In H spheres treated with the c-Met inhibitor for 2 weeks, we observed a reduction in Cyp3A activity. Whereas, HE sphere Cyp1A2 and 3A activity increased (figures 5(C) and (D)). After 4 weeks treatment, only HE sphere Cyp1A2 activity remained improved (supplementary figures 7(C) and (D)). In response to gp130 inhibition, both Cyp1A2 and Cyp3A activity was reduced in H spheres. In HE spheres. Cyp3A activity was reduced at 2 weeks onwards (figure 5(D)), with Cyp 1A2 affected at week 4. In HES spheres, cytochrome P450 activity was not significantly affected, but appeared close to baseline following gp130 inhibition for 4 weeks

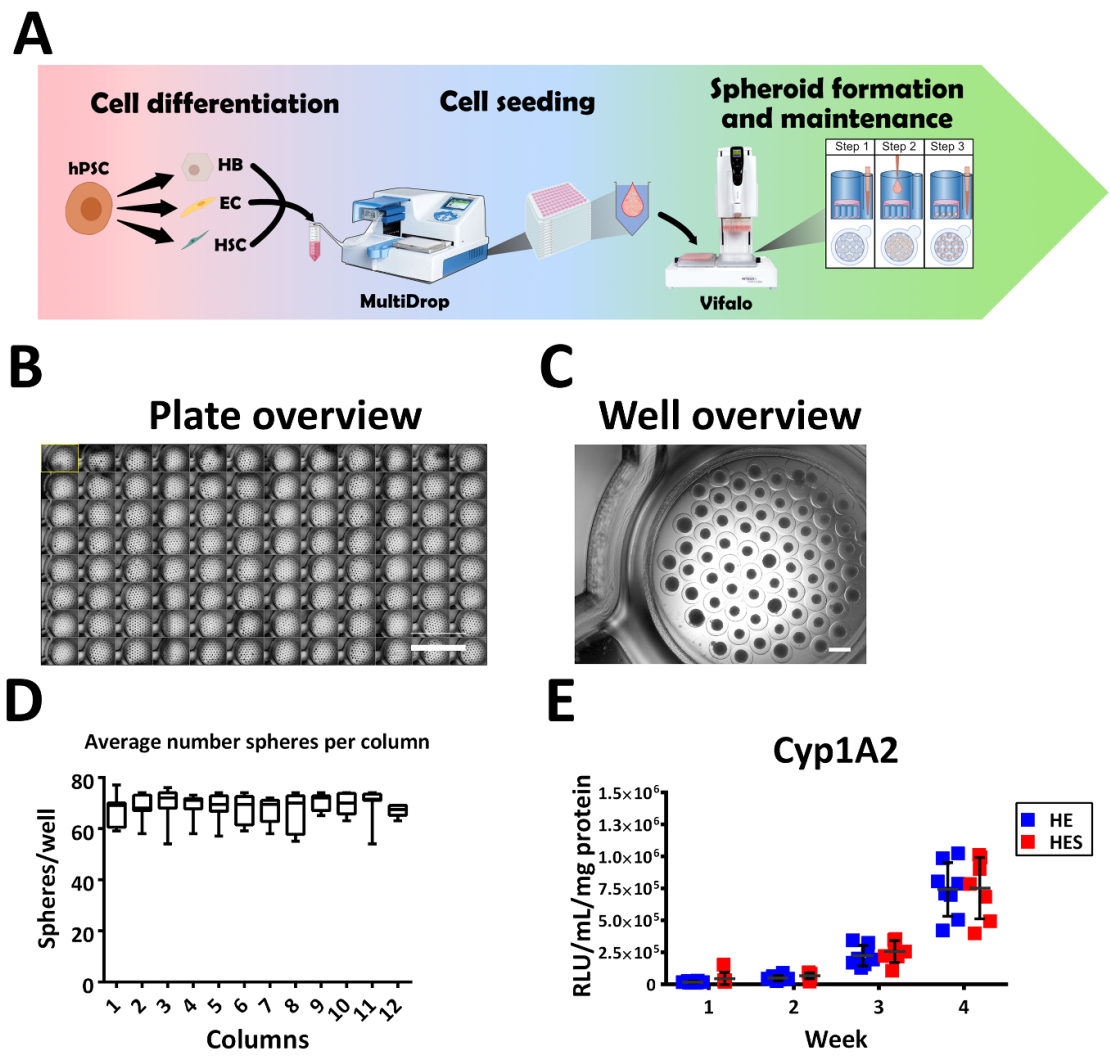

Figure 4. Automated production of human stem cell derived liver spheres. (A) Schematic representation of the production pipeline. hPSCs are differentiated into hepatic progenitors, endothelial cells and HSCs and mixed at the specified ratio (10:3:1). Next, the cell suspension containing the three cell types is dispensed into a 96-well V shape plate using the multidrop automatic liquid handling system. Finally the cells are pipetted into the microwells using the Viaflo automatic pipette. (B) Plate overview of a 96 well-plate liver spheres. Scale bar represents 10 mm (C) Well overview with liver spheres in a microwells within a 96-well plate. Scale bar represents 500 μm (D) Number of liver spheres across the plate. (mean $\pm$ SD, $n = 8$) (E) Cytochrome P450 1A2 activity from liver spheres produced by the automated pipeline analysed at different time points (mean $\pm$ SD, $n = 7$). Abbreviations: HB-Hepatic progenitor cell, EC-Endothelial cell, HSC-Hepatic stellate cells, HE-hepato-endothelial liver sphere, HES-hepato-endothelial-stellate liver sphere.

(supplementary figures 7(C) and (D)). In H spheres treated for 2 weeks with the VEGFR-2 inhibitor, we observed decreased in Cyp3A activity (figure 5(D)). However, no effects were observed at the 4 weeks time point (supplementary figures 7(C) and (D)). In H and HE spheres treated with the VEGFR-2 and -3 inhibitors for 2 weeks, we observed an increase in Cyp1A2 activity, and a decrease in Cyp3A activity (figures 5(C) and (D)). At 4 weeks inhibition, H spheres displayed decreased Cyp1A2 and 3A activity with no observed effects in HE or HES spheres (supplementary figures 7(C) and (D)). In H spheres treated with VEGF receptors 1–3 inhibitors we observed decreased in Cyp1A2 and 3A activity from 2 weeks onwards, which was not observed in HE and HES spheres (figures 5(C) and (D) and supplementary figures 7(C) and (D)).

Following the inhibitor experiments, we were keen to have a better understanding of the cellular contribution to liver sphere secretion. In these experiments, we examined the secretion of erythropoietin (EPO), the inflammatory cytokine interleukin-13 (IL-13) and the acute phase protein C-reactive protein (CRP) [30, 39]. We employed H and HES spheres for these experiments to look for differences in cell biology following exposure to a high energy 'diet' (LPO—figure 3) and TGF (Transforming growth factor)-beta, a driver of fibrosis [30]. H spheres secreted approximately 3-fold less EPO than HES spheres, indicating that endothelial and stellate cell contribution to EPO production [40, 41]. In response to both disease-mimicking environments, we observed a reduction in EPO secretion indicating loss of sphere function in HES spheres only. This was

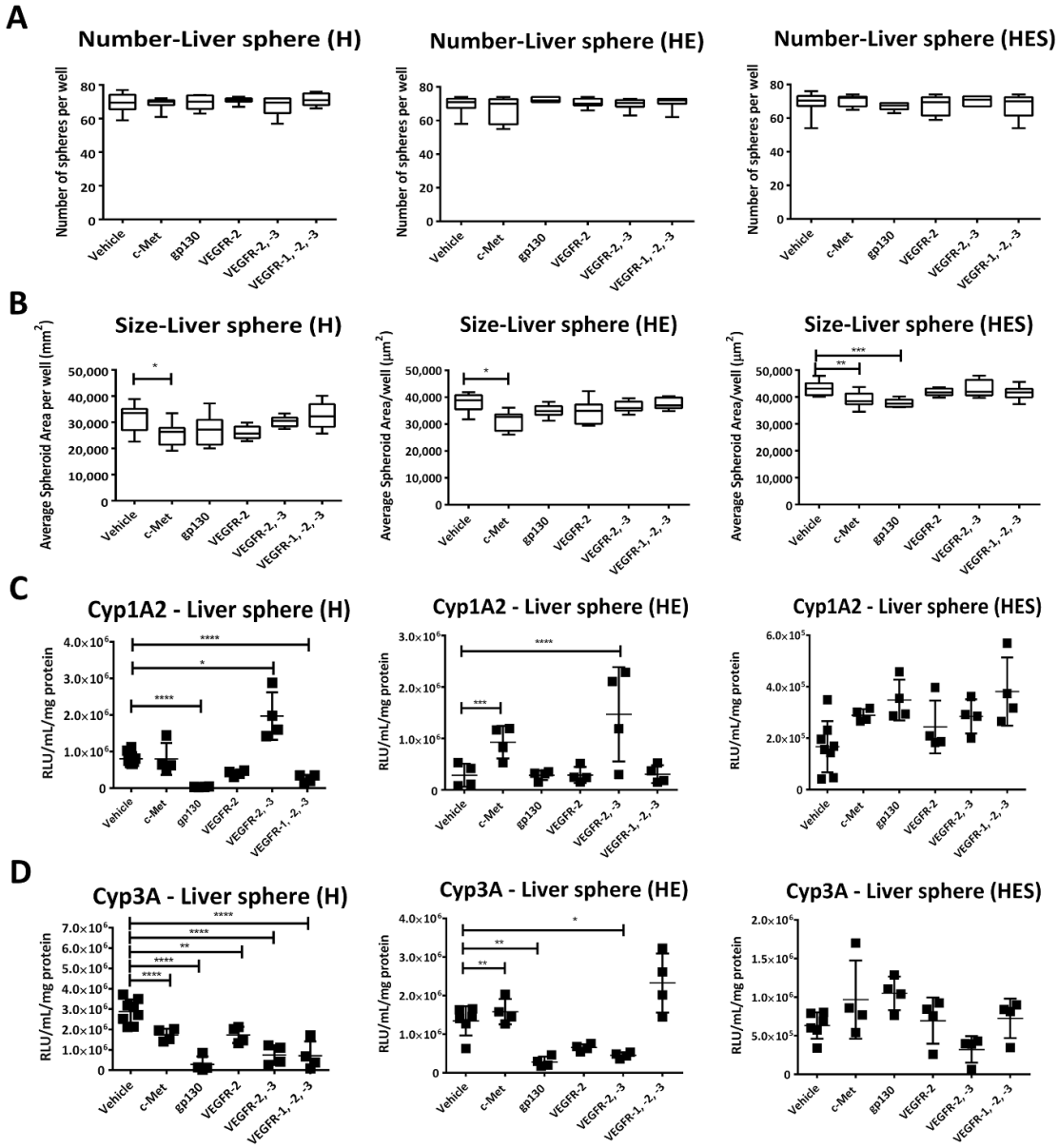

Figure 5. Determination of cell signalling involved in sphere formation, maintenance and function. Hepato liver spheres (H), hepato-endothelial liver spheres (HE) and hepato-endothelial-stellate liver spheres (HES) were produced by the automated pipeline, and incubated with inhibitors targeting key liver signalling pathways. (A) Quantification of the average sphere number per well following inhibitor exposure (box plot with mean and min-max, $n > 6$). (B) Quantification of the average sphere area per well following inhibitor exposure (box plot with mean and min-max, $n > 6$). (C) Cyp1A2 and (D) Cyp3A activity following 2 weeks inhibitor exposure (mean ± SD, $n > 4$). Data was analysed using two-way analysis of variance (ANOVA) and Tukey's multiple comparisons test ($\alpha < 0.05$).

most profound after exposure to LPO (figure 6(A)). With regard to the inflammatory chemokine, IL-13, we observed similar secretion levels between H and HES spheres when treated with vehicle (figure 6(B)). However, following TGFβ induction, but not LPO exposure, we observed an ∼2-fold increase in IL-13 secretion from only HES spheres (figure 6(B)). Finally, secretion of the acute phase protein CRP was studied. CRP secretion was increased in both H and HES spheres following LPO exposure. In contrast, only HES spheres demonstrated a significant increase in CRP secretion when exposed to TGF-β (figure 6(C)).

4. Discussion

Pluripotent stem cells represent a renewable source of human cells for tissue engineering. They are capable of large-scale expansion and differentiation into all the cell types found in the human body. This means that in theory PSCs could generate an unlimited amount of human tissue for biomedical application. While great progress has been made in the field, the scale-up and manufacture of stem cell derived tissue does require significant refinement, before industrial manufacture is possible, at an acceptable cost. In particular, the development of defined *in vitro*

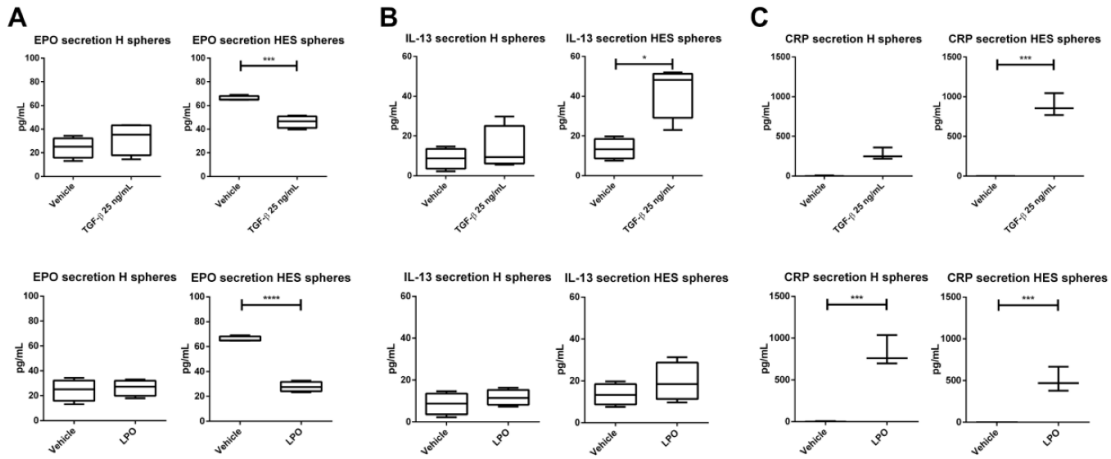

Figure 6. Increase in sphere complexity improves disease modelling *in vitro*. EPO, IL-13 and CRP secretion were analysed following LPO or TGF-β 25 ng ml^{-1} for 48 h in H and HES spheres. (A) HES spheres show an increase in basal EPO secretion with a significant decrease following both LPO and TGF-β exposure ($n = 4$). (B) Increased IL-13 induction was detected in HES spheres following TGF-β treatment only ($n = 4$). (C) CRP secretion was increased in both H and HES spheres following LPO treatment but only in HES spheres after TGF-β exposure ($n = 3$). Samples were analysed using with a one-way analysis of variance (ANOVA) ($\alpha = 0.05$) with Tukey's multiple comparisons test.

engineered cellular niches are essential to delivering a reliable piece of human tissue for biomedical application.

Our study focussed on the construction of supportive cell microenvironments which mimic key elements of organ anatomy and physiology. Central to this approach was the development of key cell-to-cell interactions that are normally found in the liver, with a focus on endothelial cells and HSCs. The endothelium plays an essential role in human liver biology during embryonic development, through to organ homeostasis in the adult. During embryonic development, before formation of functional blood vessels, endothelial cells promote the outgrowth of the hepatic progenitors from the liver bud [42]. Subsequently, the acquisition of the hepatic vasculature advances throughout embryogenesis [43]. The interplay between hepatocytes and endothelial cells has been studied extensively *in vivo* [44]. Following partial hepatectomy, hepatocytes begin to secrete VEGF, driven by hypoxia inducible factor 1. VEGF signals through liver sinusoidal endothelial cell receptors and stimulates cell proliferation, angiogenesis and secretion of liver mitogens including, hepatocyte growth factor HGF and IL-6. HGF pathway activation is mediated by the c-Met receptor, promoting hepatocyte proliferation [45]. IL-6 binds with the IL-6 receptor which subsequently forms a complex with glycoprotein 130 (gp 130), driving signal transduction and liver regeneration [46].

In addition to endothelial mesenchyme, the stellate cell also plays a vital role in the liver. HSCs reside in the liver within the space of Disse and are intimately associated with both the hepatocyte and the endothelial cell. In the healthy liver, HSC store vitamin A in lipid droplets [47]. However, following liver challenge, HSC undergo transformation to a myofibroblast state, providing the liver with an ability to respond to injury and heal certain types of damage. During normal wound healing, HSCs decrease matrix secretion and immunomodulation resulting in scar tissue resolution [47] [48]. In the context of sustained liver damage multiple proinflammatory cytokines, such as IL-6, IL-1b, tumour necrosis factor alpha (TNF-α) as well as Damage-associated molecular patterns are continually released, resulting in the chronic activation of HSCs and macrophages. This results in the prolonged secretion of pro-fibrotic signals, such as TGF-β, PDGF or angiotensin II, leading to a build-up of scar tissue which is difficult to resolve [49, 50].

Therefore, in order to build human liver tissue from pluripotent stem cells, we opted to use endothelial cell and HSC mesenchyme in our system. Stem cell derived somatic cells were produced under defined conditions (figures 1–2 and supplementary figure 5) [29–31]. The combination of stem cell derived hepatic progenitors, endothelial cells and stellate cells from the same genetic background allowed the generation of functional liver spheres (figures 2–5 and supplementary figures 2 and 7). Importantly, liver spheres were capable of modelling complex aspects of liver biology including human drug metabolism and drug overdose (figures 2–3). Additionally, liver spheres were able to model increases in lipid storage, when exposed to high-energy 'diet' and therefore may serve as a good model for studying human fatty liver disease in the future (figure 3). We also provide evidence that pancreatic cancer cell lines spontaneously interacted with liver spheres in ways that recapitulate their innate metastatic potential *in vivo* (figure 3). Although patient-derived organoids of liver metastases have been demonstrated they do not capture the early stages of metastatic seeding and

growth [51]. Our system presented here is a promising candidate to capture those early events.

Finally, we automated the production of liver spheres (figure 4). Stem cell derived liver tissue was prepared using a combination of engineering processes (figure 4). The resulting tissue was functional and reliable (figure 4) with a >2-fold reduction in variability when compared to the manual agarose microwell based system (figures 1 and 2). Given the reproducibility of the technology, we employed the automated system to investigate key liver signalling pathways involved in human liver differentiation and regeneration, combining biochemical assays and high content imaging (figure 5 and supplementary figures 6 and 7). To study the importance of signalling through c-Met, gp130 and VEGF receptors 1–3 we employed small molecule inhibitors (figure 5 and supplementary figure 7).

The inhibition of c-Met signalling for 2 weeks resulted in spheroid size reduction, likely due to reduced cell proliferation [52, 53]. The reduction in sphere size which was associated with significantly decreased Cyp activity in H spheres and increased Cyp activity in HE liver spheres. The improvement of HE sphere function, following c-Met inhibition, is in line with previous studies [54]. The modulation of Cyp P450 activity was not observed in HES liver spheres, possibly due to c-Met activation by the HSCs [55].

Following 2 weeks inhibition of gp130, we observed a similar number of liver spheres formed, but a decrease in sphere size in HES spheres only. Whilst the reduction of Cyp P450 activity was observed in H and HE spheres at this time point (figure 5 and supplementary figure 7). At 4 weeks exposure, we observed a similar number of spheres formed, but a decrease in H, HE and HES sphere size. Whereas, metabolic activity was only significantly reduced in H and HE spheres (figure 5 and supplementary figure 7). gp130 signalling has been reported to be a key driver of liver maturation and regeneration in rodents and its inhibition likely impacted on liver sphere phenotype [56, 57]. These observations reflected the importance of both gp130 and c-Met signalling in liver sphere formation and function [58, 59] (figure 5 and supplementary figure 7). Notably, we found that the more complex liver spheres were less affected by c-Met and gp130 signalling inhibition, likely due to trophic support provided in those spheres.

We then went onto study the importance of the VEGF receptor in liver sphere formation and function (figure 5 and supplementary figure 7). In response to VEGF receptor inhibition, we did not observe any changes in sphere number or size following 2 weeks treatment (figure 5). However, VEGFR-2 inhibition for 4 weeks resulted in an increase in HE and HES, but not in H sphere size (supplementary figure 7). In terms of activity, H spheres demonstrated decreased Cyp3A activity in response to VEGFR-2 inhibition at 2 weeks only. Whereas inhibition of VEGFR-2 and -3 resulted in increased Cyp1A2 activity and decreased Cyp3A activity. In response to VEGFR-1–3 inhibition, we observed reduced Cyp3A and 1A2 activity from 2 weeks onwards. In HE spheres we observed less effects of the VEGF inhibitors, with increased Cyp1A2 activity and reduced Cyp3a activity changes at 2 weeks post VEGFR-2 and -3 inhibition only. Whereas, we did not observe metabolic perturbation in HES spheres following VEGF inhibition.

Following the inhibitor studies, we examined alterations in liver sphere protein secretion. We examined EPO production, which suppresses inflammatory cytokine production [60], versus the inflammatory cytokine IL-13 and acute phase protein (CRP) production. Simple (H) and more complex spheres (HES) spheres were exposed to a high energy 'diet' (LPO—figure 3) and TGF-beta, a driver of fibrosis [30]. We observed 3-fold increased EPO secretion from HES spheres, indicating endothelial and stellate cell contribution to EPO production [40, 41]. This was significantly reduced after HES exposure to TGF-β and LPO (figure 6(A)). The reduction in EPO in HES spheres was consistent with increased production of the inflammatory cytokine IL-13, following TGF beta induction (figure 6(B)); and CRP production, following exposure to TGF-β and LPO (figure 6(C)). The response of H spheres was less robust, with CRP induction observed following LPO treatment only (figure 6(C)).

By taking an incremental approach to building liver spheres, we demonstrate the stabilising influence of endothelial and stellate cells on liver tissue phenotype (figure 5 and supplementary figure 7). In addition, we demonstrate that more complex liver spheres (HES) secrete proteins which better capture the disease environment, thereby improving our ability to study human biology *in vitro* (figure 6)

5. Conclusion

In conclusion, we have developed an automated differentiation system that permits the self-assembly of human liver tissue in vitro. Importantly, our system produces functional and phenotypically stable liver tissue, that permits the modelling of human liver biology, disease, cell signalling and protein secretion. Going forward we believe that this resource may have an important role to play in supporting failing liver function in humans.

Acknowledgments

DCH and BLV were funded by the Chief Scientist Office, reference TCS 16/37. LMM and JD were funded by CRUK core Grant A15673, C596/A17196, with special thanks to Beatson Advanced Imaging Resource and Lynn McGarry. EM was funded by an

EPSRC-SFI Centre for Doctoral Training in Engineered Tissues for Discovery, Industry and Medicine and co-supervised by Professor Manuel Salmeron-Sanchez at University of Glasgow.

Conflict of interest

Prof David Hay is a founder, director and shareholder in Stemnovate Limited

ORCID iDs

J Drew https://orcid.org/0000-0002-2864-7987
D C Hay https://orcid.org/0000-0002-7593-5973

References

[1] Zorn A M 2008 *Liver Development StemBook* (Cambridge, MA: Harvard Stem Cell Institute) http://doi.org/10.3824/stembook.1.25.1
[2] Sadri A-R, Jeschke M G and Amini-Nik S 2015 Advances in liver regeneration: revisiting hepatic stem/progenitor cells and their origin *Stem Cells Int.* **2016** 7920897
[3] Miyajima A, Tanaka M and Itoh T 2014 Stem/progenitor cells in liver development, homeostasis, regeneration, and reprogramming *Cell Stem Cell* **14** 561–74
[4] Kadyk L C, Collins L R, Littman N J and Millan M T 2015 Proceedings: moving toward cell-based therapies for liver disease *Stem Cells Transl. Med.* **4** 207–10
[5] DiMasi J A, Grabowski H G and Hansen R W 2016 Innovation in the pharmaceutical industry: new estimates of R&D costs *J. Health Econ.* **47** 20–33
[6] Mohs R C and Greig N H 2017 Drug discovery and development: role of basic biological research *Alzheimers Dement* **3** 651–7
[7] Harrison R K 2016 Phase II and phase III failures: 2013–2015 *Nat. Rev. Drug Discov.* **15** 817–8
[8] Onakpoya I J, Heneghan C J and Aronson J K 2016 Post-marketing withdrawal of 462 medicinal products because of adverse drug reactions: a systematic review of the world literature *BMC Med.* **14** 10
[9] Soldatow V Y, Lecluyse E L, Griffith L G and Rusyn I 2013 In vitro models for liver toxicity testing *Toxicol. Res.* **2** 23–39
[10] Gómez-Lechón M J, Tolosa L, Conde I and Donato M T 2014 Competency of different cell models to predict human hepatotoxic drugs *Expert Opin. Drug Metab. Toxicol.* **10** 1553–68
[11] Meseguer-Ripolles J, Khetani S R, Blanco J G, Iredale M and Hay D C 2017 Pluripotent stem cell-derived human tissue: platforms to evaluate drug metabolism and safety *AAPS J.* **20** 20
[12] Szkolnicka D and Hay D*et al* 2020 Liver stem cells *Principles of Tissue Engineering*, ed R Lanza, R Langer, J Vacanti and A Atala 5th edn ch 40 (Amsterdam: Elsevier)
[13] Rashid S T *et al* 2010 Modeling inherited metabolic disorders of the liver using human induced pluripotent stem cells *J. Clin. Invest.* **120** 3127–36
[14] Cayo M A *et al* 2017 A drug screen using human iPSC-derived hepatocyte-like cells identifies cardiac glycosides as a potential treatment for hypercholesterolemia *Cell Stem Cell* **20** 478–489.e5
[15] Graffmann N, Ring S, Kawala M-A, Wruck W, Ncube A, Trompeter H-I and Adjaye J 2016 Modeling nonalcoholic fatty liver disease with human pluripotent stem cell-derived immature hepatocyte-like cells reveals activation of PLIN2 and confirms regulatory functions of peroxisome proliferator-activated receptor alpha *Stem Cells Dev.* **25** 1119–33
[16] Lyall M J *et al* 2018 Modelling non-alcoholic fatty liver disease in human hepatocyte-like cells *Phil. Trans. R. Soc.* B **373** 20170362
[17] Szkolnicka D, Farnworth S L, Lucendo-Villarin B, Storck C, Zhou W, Iredale J P, Flint O and Hay D C 2014 Accurate prediction of drug-induced liver injury using stem cell-derived populations *Stem Cells Transl. Med.* **3** 141–8
[18] Lucendo-Villarin B, Filis P, Swortwood M J, Huestis M A, Meseguer-Ripolles J, Cameron K, Iredale J P, O'Shaughnessy P J, Fowler P A and Hay D C 2017 Modelling foetal exposure to maternal smoking using hepatoblasts from pluripotent stem cells *Arch. Toxicol.* **91** 3633–43
[19] Meseguer-Ripolles J, Lucendo-Villarin B, Wang Y and Hay D C 2018 Semi-automated production of hepatocyte like cells from pluripotent stem cells *J. Vis. Exp.* **137** 57995
[20] Pineda E T, Nerem R M and Ahsan T 2013 Differentiation patterns of embryonic stem cells in two versus three dimensional culture *Cells Tissues Organs* **197** 399–410
[21] Nigam S K 2015 What do drug transporters really do? *Nat. Rev. Drug Discov.* **14** 29–44
[22] Albrecht W *et al* 2019 Prediction of human drug-induced liver injury (DILI) in relation to oral doses and blood concentrations *Arch. Toxicol.* **93** 1609–37
[23] Rashidi H, Alhaque S, Szkolnicka D, Flint O and Hay D C 2016 Fluid shear stress modulation of hepatocyte-like cell function *Arch. Toxicol.* **90** 1757–61
[24] Rashidi H *et al* 2018 3D human liver tissue from pluripotent stem cells displays stable phenotype in vitro and supports compromised liver function in vivo *Arch. Toxicol.* **92** 3117–29
[25] Takebe T *et al* 2013 Vascularized and functional human liver from an iPSC-derived organ bud transplant *Nature* **499** 481–4
[26] Takebe T *et al* 2017 Massive and reproducible production of liver buds entirely from human pluripotent stem cells *Cell Rep.* **21** 2661–70
[27] Ouchi R *et al* 2019 Modeling steatohepatitis in humans with pluripotent stem cell-derived organoids *Cell Metab.* **30** 374-384.e6
[28] Wang Y, Alhaque S, Cameron K, Meseguer-Ripolles J, Lucendo-Villarin B, Rashidi H and Hay D C 2017 Defined and scalable generation of hepatocyte-like cells from human pluripotent stem cells *J. Vis. Exp.* **121** 55355
[29] MacAskill M G *et al* 2018 Robust revascularization in models of limb ischemia using a clinically translatable human stem cell-derived endothelial cell product *Mol. Ther.* **26** 1669–84
[30] Liu Y, Munker S, Müllenbach R and Weng H-L 2012 IL-13 Signaling in liver fibrogenesis *Front. Immunol.* **3** 116
[31] Lucendo-Villarin B, Rashidi H, Alhaque S, Fischer L, Meseguer-Ripolles J, Wang Y, O'Farrelly C, Themis M and Hay D C 2019 Serum free production of three-dimensional human hepatospheres from pluripotent stem cells *J. Vis. Exp.* **149** e59965
[32] Dekkers J F *et al* 2019 High-resolution 3D imaging of fixed and cleared organoids *Nat. Protocols* **14** 1756–71
[33] Szkolnicka D, Lucendo-Villarin B, Moore J K, Simpson K J, Forbes S J and Hay D C 2016 Reducing hepatocyte injury and necrosis in response to paracetamol using noncoding RNAs *Stem Cells Transl. Med.* **5** 764–72
[34] Valderrama-Treviño A I, Barrera-Mera B, Ceballos-Villalva J C and Montalvo-Javé E E 2017 Hepatic metastasis from colorectal cancer *Euroasian J. Hepatogastroenterol.* **7** 166–75
[35] Miarka L *et al* 2019 The hepatic microenvironment and TRAIL-R2 impact outgrowth of liver metastases in pancreatic cancer after surgical resection *Cancers* **11** 745
[36] Papalazarou V, Zhang T, Paul N R, Juin A, Cantini M, Maddocks O D K, Salmeron-Sanchez M and Machesky L M 2020 The creatine–phosphagen system is mechanoresponsive in pancreatic adenocarcinoma and fuels invasion and metastasis *Nat. Metab.* **2** 62–80

[37] Lee J S, Semela D, Iredale J and Shah V H 2007 Sinusoidal remodeling and angiogenesis: A new function for the liver-specific pericyte? *Hepatology* **45** 817–25
[38] Coll M *et al* 2018 Generation of hepatic stellate cells from human pluripotent stem cells enables in vitro modeling of liver fibrosis *Cell Stem Cell* **23** 101–13.e7
[39] Anagnostou A, Lee E S, Kessimian N, Levinson R and Steiner M 1990 Erythropoietin has a mitogenic and positive chemotactic effect on endothelial cells *PNAS* **87** 5978–82
[40] Maiese K, Li F and Chong Z Z 2005 New avenues of exploration for erythropoietin *JAMA* **293** 90–95
[41] Tan K S, Kulkeaw K, Nakanishi Y and Sugiyama D 2017 Expression of cytokine and extracellular matrix mRNAs in fetal hepatic stellate cells *Genes Cells* **22** 836–44
[42] Matsumoto K, Yoshitomi H, Rossant J and Zaret K S 2001 Liver organogenesis promoted by endothelial cells prior to vascular function *Science* **294** 559–63
[43] Gouysse G, Couvelard A, Frachon S, Bouvier R, Nejjari M, Dauge M C, Feldmann G, Hénin D and Scoazec J Y 2002 Relationship between vascular development and vascular differentiation during liver organogenesis in humans *J. Hepatol.* **37** 730–40
[44] Preziosi M E and Monga S P 2017 Update on the mechanisms of liver regeneration *Semin. Liver Dis.* **37** 141–51
[45] Borowiak M, Garratt A N, Wüstefeld T, Strehle M, Trautwein C and Birchmeier C 2004 Met provides essential signals for liver regeneration *Proc. Natl. Acad. Sci. USA* **101** 10608–13
[46] Schmidt-Arras D and Rose-John S 2016 IL-6 pathway in the liver: from physiopathology to therapy *J. Hepatol.* **64** 1403–15
[47] Tsuchida T and Friedman S L 2017 Mechanisms of hepatic stellate cell activation *Nat. Rev. Gastroenterol. Hepatol.* **14** 397–411
[48] Forbes S J and Newsome P N 2016 Liver regeneration—mechanisms and models to clinical application *Nat. Rev. Gastroenterol. Hepatol.* **13** 473–85
[49] Chang J *et al* 2013 Activated hepatic stellate cells mediate the differentiation of macrophages *Hepatol. Res.* **43** 658–69
[50] Pellicoro A, Ramachandran P, Iredale J P and Fallowfield J A 2014 Liver fibrosis and repair: immune regulation of wound healing in a solid organ *Nat. Rev. Immunol.* **14** 181–94
[51] Boj S F *et al* 2015 Organoid models of human and mouse ductal pancreatic cancer *Cell* **160** 324–38
[52] Bouattour M, Raymond E, Qin S, Cheng A-L, Stammberger U, Locatelli G and Faivre S 2018 Recent developments of c-Met as a therapeutic target in hepatocellular carcinoma *Hepatology* **67** 1132–49
[53] Ielasi L, Tovoli F and Piscaglia F 2019 Lenvatinib mesylate to treat hepatocellular carcinoma *Drugs Today* **55** 305
[54] Donato M T, Gómez-Lechón M J, Jover R, Nakamura T and Castell J V 1998 Human hepatocyte growth factor down-regulates the expression of cytochrome P450 isozymes in human hepatocytes in primary culture *J. Pharmacol. Exp. Ther.* **284** 760–7
[55] Kubota H, Yao H and Reid L M 2007 Identification and characterization of vitamin A-storing cells in fetal liver: implications for functional importance of hepatic stellate cells in liver development and hematopoiesis *Stem Cells* **25** 2339–49
[56] Kamiya A *et al* 1999 Fetal liver development requires a paracrine action of oncostatin M through the gp130 signal transducer *Embo J.* **18** 2127–36
[57] Modares N F *et al* 2019 IL-6 Trans-signaling controls liver regeneration after partial hepatectomy *Hepatology* **70** 2075–91
[58] Ishikawa T, Factor V M, Marquardt J U, Raggi C, Seo D, Kitade M, Conner E A and Thorgeirsson S S 2012 Hepatocyte growth factor/c-met signaling is required for stem-cell–mediated liver regeneration in mice *Hepatology* **55** 1215–26
[59] Marquardt J U, Seo D, Gómez-Quiroz L E, Uchida K, Gillen M C, Kitade M, Kaposi-Novak P, Conner E A, Factor V M and Thorgeirsson S S 2012 Loss of c-Met accelerates development of liver fibrosis in response to CCl(4) exposure through deregulation of multiple molecular pathways *Biochim. Biophys. Acta* **1822** 942–51
[60] Nairz M, Sonnweber T, Schroll A, Theurl I and Weiss G 2012 The pleiotropic effects of erythropoietin in infection and inflammation *Microbes Infect.* **3** 238–46